

Collision of Comet Shoemaker-Levy 9 with Jupiter Observed by the NASA Infrared Telescope Facility

G. Orton, M. A'Hearn, K. Baines, D. Deming, T. Dowling, J. Goguen, C. Griffith, H. Hammel, W. Hoffmann, D. Hunten, D. Jewitt, T. Kostiuik, S. Miller, K. Noll, K. Zahnle, N. Achilleos, A. Dayal, L. Deutsch, F. Espenak, P. Esterle, J. Friedson, K. Fast, J. Harrington, J. Hora, R. Joseph, D. Kelly, R. Knacke, J. Lacy, C. Lisse, J. Rayner, A. Sprague, M. Shure, K. Wells, P. Yanamandra-Fisher, D. Zipoy, G. Bjoraker, D. Buhl, W. Golisch, D. Griep, C. Kaminski, C. Arden, A. Chaikin, J. Goldstein, D. Gilmore, G. Fazio, T. Kanamori, H. Lam, T. Livengood, M.-M. MacLow, M. Marley, T. Momary, D. Robertson, P. Romani, J. Spitale, M. Sykes, J. Tennyson, D. Wellnitz, S.-W. Ying

The National Aeronautics and Space Administration (NASA) Infrared Telescope Facility was used to investigate the collision of comet Shoemaker-Levy 9 with Jupiter from 12 July to 7 August 1994. Strong thermal infrared emission lasting several minutes was observed after the impacts of fragments C, G, and R. All impacts warmed the stratosphere and some the troposphere up to several degrees. The abundance of stratospheric ammonia increased by more than 50 times. Impact-related particles extended up to a level where the atmospheric pressure measured several millibars. The north polar near-infrared aurora brightened by nearly a factor of 5 a week after the impacts.

Many of the extraordinary events surrounding the impact of comet Shoemaker-Levy 9 with Jupiter were observed from the NASA Infrared Telescope Facility (IRTF) from 12 July to 7 August 1994 (1). Scientific goals included characterization of the cometary fragments under the influence of Jupiter's electromagnetic environment; measurement of the impact radiation; measurement of temperature, chemistry, and particulate properties at the impact sites and their time evolution; determination of changes in the ring system in the increased dust environment; and detection of various waves and oscillations (2).

Up to three instruments could be mounted simultaneously at the Cassegrain focus in a manner that allowed them to be exchanged quickly, minimizing replacement requirements. The instruments chosen for the observing campaign were NSFCAM, a

camera and low-resolution spectrometer for wavelengths of $\lambda = 1$ to $5 \mu\text{m}$ (3), CSHELL, a 1- to $5\text{-}\mu\text{m}$ high-resolution array spectrometer and imager (4), MIRAC2, a 2- to $21\text{-}\mu\text{m}$ array camera (5), and IRSHELL, a 5- to $23\text{-}\mu\text{m}$ high-resolution array spectrometer (6). At the Coudé focus, the Goddard Infrared Heterodyne Spectrometer (IRHS) provided the highest spectral resolution in the 10- to $12\text{-}\mu\text{m}$ spectral region ($\lambda/\Delta\lambda \approx 10^6$) (7).

Fragments and Ring

Fragments K, R, and Q1 were undetectable above the noise limit at $1.25 \mu\text{m}$ a week before impact even though they had been detected at the IRTF the preceding January and May at the same wavelength with similar system sensitivity and noise. A week before impact, they were all just inside the

nominal edge of the jovian magnetosphere, some 70 jovian radii from the planet. If most of the $1.25\text{-}\mu\text{m}$ radiation from the comet was contributed by scattering from the dust in the tail, then this result is consistent with the absence of tails in several fragments at $0.89 \mu\text{m}$, as reported by Jewitt and Kalas (8). The cometary dust may have been removed by electrical charging in the magnetosphere, followed by dispersal driven by the Lorentz force produced as it crossed Jupiter's magnetic field or by disruption caused by electrostatic repulsion. Preliminary analysis of observations made of Jupiter's ring at $2.26 \mu\text{m}$ shows no change between May and August of 1994, ruling out any short-term input of dust to the rings or cometary dust-ring dust collisions.

Impacts

Table 1 summarizes the detections and non-detections of the impacts of fragments B, C, F, G, R, V, and W. Before the impact of fragment C, we imaged Io, Europa, and the impact site simultaneously, but the brightnesses of the two satellites remained constant to within 1.5%, with no convincing evidence for any reflection of impact radiation greater than $2 \times 10^{-17} \text{ W cm}^{-2} \mu\text{m}^{-1}$, which should have been orders of magnitude higher for Io than Europa as a result of their different scattering geometries. The impact-generated radiation from fragment C was visible near the remnant site of fragment A, whose impact was one jovian rotation period earlier (Fig. 1). The light curve for the C impact shows significant structure on time scales of about 1 min while rising to a peak brightness of approximately $1 \times 10^{-15} \text{ W cm}^{-2} \mu\text{m}^{-1}$, some 80% of the brightness of Io (Fig. 2). The brightness then fell exponentially to a constant level of 3% of the maximum.

After the successful measurement of the C impact radiation at a single wavelength, we tried to measure subsequent impacts at two wavelengths to characterize the evolution of both temperature and solid angle for the emission source. We wanted to differentiate between continuum emission from

G. Orton, K. Baines, J. Goguen, J. Friedson, and P. Yanamandra-Fisher are at the Jet Propulsion Laboratory, California Institute of Technology, Pasadena, CA 91109, USA. M. A'Hearn, P. Esterle, K. Fast, D. Zipoy, and D. Wellnitz are in the Astronomy Department, University of Maryland, College Park, MD 20742, USA. D. Deming, T. Kostiuik, F. Espenak, C. Lisse, G. Bjoraker, D. Buhl, T. Livengood, and P. Romani are at NASA Goddard Space Flight Center, Greenbelt, MD 20771, USA. T. Dowling, H. Hammel, and J. Harrington are at Massachusetts Institute of Technology, Cambridge, MA 02139, USA. C. Griffith is in the Department of Physics and Astronomy, Northern Arizona University, Flagstaff, AZ 86011, USA. W. Hoffmann and A. Dayal are at Steward Observatory, University of Arizona, Tucson, AZ 85721, USA. D. Hunten, A. Sprague, K. Wells, and M. Sykes are at the Lunar and Planetary Laboratory, University of Arizona, Tucson, AZ 85721, USA. D. Jewitt, J. Hora, R. Joseph, J. Rayner, M. Shure, W. Golisch, D. Griep, and C. Kaminski are at the Institute for Astronomy, University of Hawaii, Honolulu, HI 96822, USA. S. Miller, N. Achilleos, H. Lam, and J. Tennyson are in the Department of Physics and Astronomy, University College, London WC1E 6BT, UK. K. Noll and D. Gilmore are at the Space Telescope Science Institute, Baltimore, MD 21218, USA. K. Zahnle is at NASA Ames Research Center, Moffet Field, CA 94053, USA. L. Deutsch is in the Five College Astronomy Department, University of Massachusetts, Amherst, MA 01003, USA. D. Kelly and J. Lacy are in the Department of Astronomy, University of Texas, Austin, TX 78712, USA. R. Knacke is at the Pennsylvania State University, Erie, PA 16563, USA. C. Arden is at Trinity Hall, Cambridge CB2 1TJ, UK. A. Chaikin is in the Department of Physics, St. Andrews University, Fife, Scotland. J. Goldstein is at the National Air and Space Museum, Washington, DC 20560, USA. G. Fazio is at the Smithsonian Astrophysical Observatory, Cambridge, MA 02138, USA. T. Kanamori is in the Department of Mechanical Engineering and Design, Stanford University, Stanford, CA 94305, USA. M.-M. MacLow is in the Department of Astronomy and Astrophysics, University of Chicago, Chicago, IL 60637, USA. M. Marley is in the Department of Astronomy, New Mexico State University, Las Cruces, NM 88003, USA. T. Momary is at the University of California, Los Angeles, CA 90024, USA. D. Robertson is in the Department of Physics and Astronomy, Leicester University, Leicester LE1 7RH, UK. J. Spitale is at California Institute of Technology, Pasadena, CA 91126, USA. S.-W. Ying is at the Imperial College of Science, Technology, and Medicine, London SW7 2BZ, UK.

hot particles and possible line emission or reflected sunlight at 2.295 μm by comparing them with 4.79- μm radiation, a wavelength at which Jupiter's atmosphere is transparent, and at which reflected sunlight is minimized. On 18 July, heavy fog kept us from opening the dome except between 7:35 and 8:09 UT, during which time the 4.78- μm signal became so bright that it saturated the detectors (Fig. 3). The bright emission at this wavelength suggests that continuum thermal emission made up a major component of the signal.

The impact of fragment R was sequentially sampled at three thermal infrared wavelengths (Table 1). The first unambiguous evidence for excess infrared radiation from the impact appeared in a 7.85- μm image taken at 5:40:57 UT; the radiation reached a peak at each wavelength at about 5:44:30 UT (Fig. 4). Flux calibration is incomplete, but provisional estimates for the peak excess fluxes are 9×10^{-15} , 4×10^{-15} , and $2 \times 10^{-15} \text{ W cm}^{-2} \mu\text{m}^{-1}$ at 7.85, 10.30, and 12.20 μm , respectively. At 10.30 μm , excess fluxes were clearly sustained at 10% of the peak for at least 40 min after the initial

detection. At 7.85 and 12.20 μm , the excess flux seemed to decay to near preimpact values within 30 min after the initial detection, although we saw clear evidence for the residual impact sites at these wavelengths at later times.

Thermal emission, rather than reflected sunlight, is most likely the dominant source of the infrared flux. To match the peak brightness of the R fragment signal at 10.30 μm , a unit-albedo Lambert disk reflecting sunlight would have to be larger than Jupiter. Because the signal from fragment C is 80% as bright as that from Io, a high-albedo satellite at 2.248 μm , an optically thick cloud of high-albedo particles about 3000 km in diameter, the same size as Io, would be required to match the measured C fireball flux and would be as bright as Io at visible wavelengths. Obviously, no such large-scale structure is seen in Earth-based images (9). The similarity of the gross structure of the C and R light curves, despite their large wavelength difference, also suggests that both have a similar thermal origin. If fragment C entered Jupiter's atmosphere at 7:13:51 \pm 0:18 UT as seen from Earth (9), then the

time delay between entry and the observed peak emission was 9 ± 3 min. If fragment R entered Jupiter's atmosphere at 5:34:30 UT (10), then the time delay between entry and observed peak emission was 10 min. This delay is most likely a combination of the time required for the impact site and the upwelling fireball to rotate into direct view from the Earth, combined with the trajectory time for the material that was raised up in the fireball to reenter and heat the upper atmosphere.

Atmospheric Temperatures

We measured the temperature field using techniques similar to those used in earlier work on Jupiter's global temperatures (11), choosing thermal infrared wavelengths

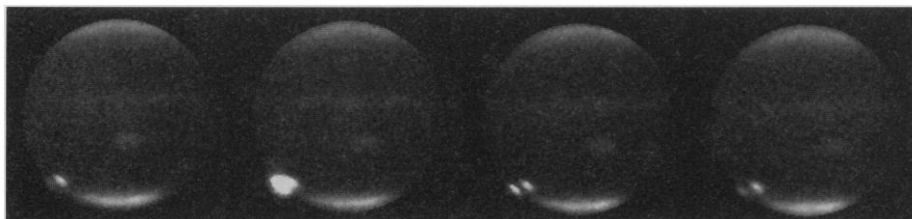


Fig. 1. Images of Jupiter at 2.248 μm taken with NSFCAM on 17 July 1994 (UT). Times, to the nearest minute, are 7:15, 7:21, 7:27, and 7:34 UT, left to right. The north and south polar hazes are visible in each image, as is the particulate feature associated with the impact of fragment A. By 7:40 UT, the C fragment had nearly assumed its asymptotic appearance as a particulate feature merely reflecting sunlight from the atmosphere similar to and slightly fainter than the A fragment particulate feature.

Table 1. Summary of impact observations.

Fragment	Instrument	Wavelength (width) (μm)	UT date and time	Sample time (s)	Weather and comments
B	MIRAC2	2.2 (0.2)	17 July 2:36 to 3:07	4	Clear; no obvious effect of impact
C	NSFCAM	2.248 (0.022)	17 July 6:53 to 7:15	3	Clear; Io, Europa, and jovian limb observed; Less than 1 to 5% change in satellite brightness
			7:15 to 7:44	3	Clear; detailed light curve of impact showing structure (Figs. 1 and 2)
F	MIRAC2	10.30 (0.21)	18 July 0:25 to 0:53	16	Some clouds; no obvious effect of impact
G*	NSFCAM	2.295 (0.046) 4.78 (0.24)	18 July 7:35 to 8:09	13	Some fog and clouds; some data, detector saturation (Fig. 3)
			21 July 5:08 to 6:20	17	Some clouds; detailed light curve at 3 wavelengths (Fig. 4)
V	CSHELL	—	22 July	—	Clouds; no data
W	NSFCAM	—	22 July	—	Clouds; no data

*For these observations, we cycled between filters sequentially; sample times shown represent times between different filters. For the MIRAC2 R fragment observations, measurements were made more often at 7.85 μm after 5:55 UT.

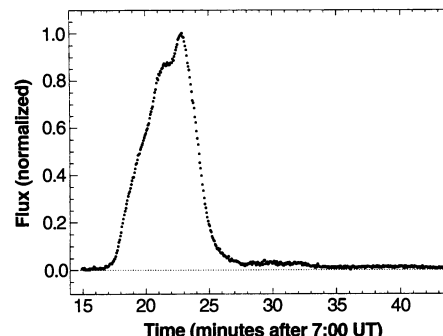


Fig. 2. Normalized light curve for the C fragment impact fireball observed with NSFCAM at a wavelength of 2.248 μm .

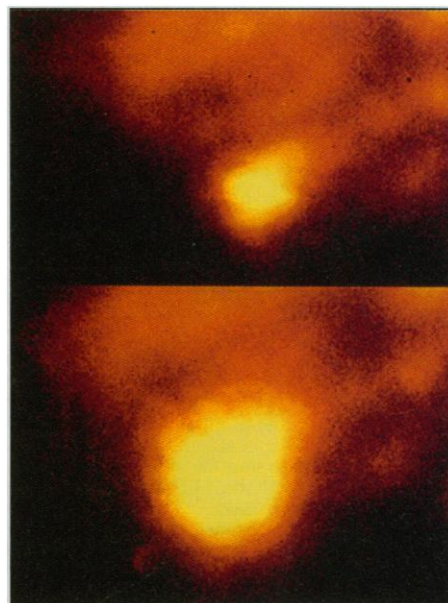


Fig. 3. Images of the G fragment impact fireball taken with NSFCAM in a filter at $4.78 \pm 0.11 \mu\text{m}$ (known as the narrow-band M filter) on 18 July 1994 at (top) 7:39:45 and (bottom) 7:41:41 UT. Only the southwestern limb of Jupiter is visible. The dramatic increase in the plume brightness is evident in these images.

dominated by the opacity of well-mixed gases. At $7.85\ \mu\text{m}$, where strong CH_4 lines emit thermal radiation from the stratosphere near 10-mbar pressure, the E impact site (Fig. 5) was as much as 1.5 K warmer than its surroundings and roughly 20,000 km in diameter. The Q1 and R impact sites were 3 to 4 K warmer than their surroundings within 10 hours of their impacts. The large extent of these warm areas offers circumstantial evidence that warm particles and gases deposited by the descending impact ejecta were responsible for their heating. The absence of enhanced emission at nearby $8.57\ \mu\text{m}$ makes it far more likely that the $7.85\text{-}\mu\text{m}$ emission arose from higher kinetic temperatures rather than thermal emission from enhanced particulate abundances, unless special spectral properties for the particles are invoked. By 21 July, the E impact site had cooled to less than 0.5 K warmer than its surroundings (Fig. 5). The L site, 2 K warmer than its surroundings on 20 July, had cooled by $\sim 1\ \text{K}$ 19 hours later. This time scale for cooling, on the order of

2 days, is much shorter than radiative cooling by the ambient gases (12); it most likely implies increased thermal emission and subsequent radiative cooling by the elevated particle population at impact sites.

Observations sensitive to tropospheric temperatures at levels with pressures between 150 and 400 mbar were made at 13.0, 17.2, 17.8, and $20.8\ \mu\text{m}$, where the opacity of the atmosphere is dominated by molecular hydrogen. On 21 July, the tropospheric temperatures at 150 and 400 mbar, measured at 17.2 and $13.0\ \mu\text{m}$, respectively, were 4 and 1.3 K higher than their surroundings (Fig. 6). On the other hand, the E impact site, observed within 13 hours of impact, showed a barely discernible temperature increase. The perturbations in the 400-mbar temperature were rapidly convected away (Fig. 6), but the perturbation in the 150-mbar temperature of the L impact site was still 1.5 to 2.5 K above the surrounding temperature 2 weeks later. This is still shorter than the normal radiative decay time and implies

either particulate-enhanced radiation or advection as the likely mechanisms for restoring temperatures.

Atmospheric Chemistry

One of the most notable discoveries was that of enhanced NH_3 gas in Jupiter's stratosphere over impact sites. Figure 7 clearly shows a strong maximum signal over the L impact site from emission arising from the center of a strong NH_3 spectral line near 50- to 100-mbar total pressure and emission from a nearby continuum arising from 300-mbar pressure. The spectrum of a nearby nonimpact region (Fig. 8) can be modeled by the same temperature structure that was fit to this region in 1989 (13) and by a NH_3 mixing ratio equivalent to 40% of the NH_3 saturated vapor pressure up through the temperature minimum (near $\sim 100\text{-mbar}$ pressure). Above this, the NH_3 mixing ratio cannot exceed 2 parts per billion (ppb) because of stratospheric photochemical destruction. However, at the fragment K impact site, the NH_3 emission feature in Fig. 8 is matched by raising the NH_3 stratospheric mixing ratio to 80 ppb, a value close to the fully saturated mixing ratio at a temperature minimum of 111 K, close to the nonimpact site value. The radiance at the cusp between the NH_3 absorption and emission can be matched either by raising the temperature minimum by 7 K or by adding a continuum emission, which could arise from stratospheric particulates. The other emission line in Fig. 8 at $907.74\ \text{cm}^{-1}$ arises from C_2H_4 with a stratospheric mixing ratio of 3 ppb.

The IRHS also observed NH_3 injected into the stratosphere at the Q1 impact site, measuring a strong line at $892.1577\ \text{cm}^{-1}$ (Fig. 9). With temperature profiles that are constrained by the IRHS measurements of C_2H_6 (14), implying a maximum temperature of 180 K, the data can be fit by a uniform stratospheric NH_3 mixing ratio of 10 ppb. For a stratospheric temperature profile 10 K warmer, the NH_3 mole fraction fitting the data would be about a factor of 5 lower. These abundances are well below the saturation level for stratospheric temperatures. Measurements of the line shape and width show that the line emission originated in the pressure regime of 1 to 30 mbar, implying that impact-enhanced NH_3 gas is distributed at least this high. Measurements centered 8° in longitude away from the Q1 impact site yielded an upper limit of 2 ppb for the NH_3 mole fraction, with a precision of about 30%.

Broader band images by MIRAC2 at $10.74\ \mu\text{m}$ showed enhanced NH_3 emission over nearly every impact site. The decay of this emission from 17 July to 6 August is consistent with the rate of photochemical

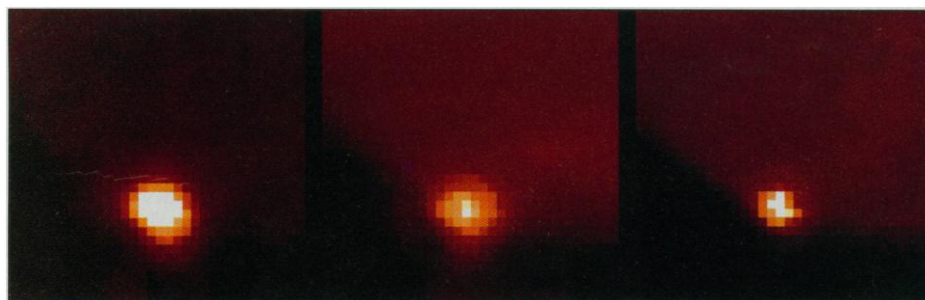


Fig. 4. Images of the R fragment impact fireball taken with MIRAC2 on 21 July 1994 in three filters, centered on 5:42 UT. The observations were taken sequentially, 17 s apart, at wavelengths $7.85\ \mu\text{m}$ (left), $10.30\ \mu\text{m}$ (center), and $12.20\ \mu\text{m}$ (right). The images are stretched logarithmically to show Jupiter and the impact-related brightening at the same time. The impact radiation was not spatially resolved at this time.

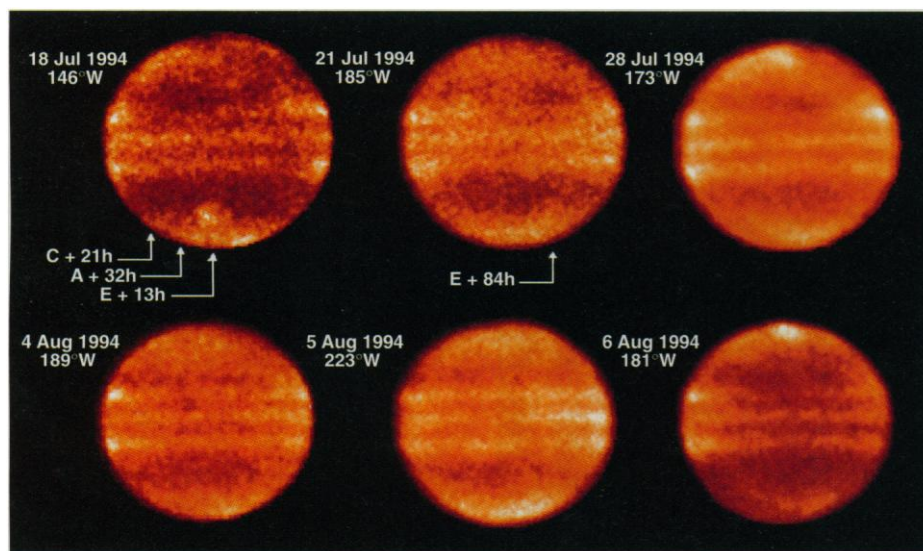


Fig. 5. Images of Jupiter's thermal emission at $7.85\ \mu\text{m}$. The images, identified by the UT date and System III longitude of the central meridian, were chosen to present nearly the same Earth-facing hemisphere to show the evolution of stratospheric temperatures at several impact sites over time.

destruction expected near 10 mbar, where photolysis alone should reduce the NH_3 abundance by a factor of at least 6 in about a week.

Figure 10 shows a CSHELL spectrum with a weak CO line that is most probably the result of narrow CO emission filling in the center of the broader CO absorption line that is spectrally resolved. The presence of CO emission 10 days after the impacts implies that it must be relatively high in the stratosphere, at 10^{-5} bar or less, where the temperature may be warm enough ($T \geq 280$ K) to produce observable emission if CO was enhanced at the impact sites (15). Carbon monoxide is the reservoir

for oxygen, normally rare in Jupiter's upper troposphere and stratosphere, and it is most likely distributed with a uniform mixing ratio of 1 ppb throughout the preimpact stratosphere. The impact of even a modest (10^{15} g) comet would have increased this small amount of CO substantially, both directly from CO in the comet itself and indirectly from any other oxygen-containing material in the comet, such as H_2O , that is eventually converted to CO. This observation provides some evidence that the impacts provided some small stratospheric enhancement of the ordinarily stable CO molecule.

Further analysis will be required to re-

trieve upper limits for targeted but undetected molecules. Such molecules include H_2O and H_2S , which might arise from the upwelling of tropospheric gas, and HCN, which might have been created as a part of impact shock chemistry.

Atmospheric Particulates

Atmospheric particulates and aurora were investigated with NSFCAM, which sampled 17 wavelengths, four of which are shown in Fig. 11. These images show particulates at most impact sites, including images in strong $3.41\text{-}\mu\text{m}$ CH_4 absorption, which is sensitive to sunlight reflected from particles at pressures of 3 mbar or less. Before the impacts, only emission from H_3^+ aurorae near the poles and a faint auroral glow over the rest of the planet were detectable at this wavelength. At the shorter wavelengths where CH_4 absorption is still present but weaker, the impact sites of fragments K, H, Q1, G, R, and L are many times brighter than the polar hazes and the Great Red Spot, indicating that particulates at impact sites at pressures of less than several millibars were more numerous or more reflective than particulates in the other jovian features. On the other hand, there was no sign of the impact sites in the $1.60\text{-}\mu\text{m}$ images, which are sensitive to the reflectivities of the deepest clouds, implying that the difference in absorption optical depth between particles at the impact sites and the rest of the atmosphere is quite low in the near infrared, in contrast to the visible and near ultraviolet (9).

The core brightnesses of the G, L, and Q1 features did not change more than our 10% level of uncertainty, but the brightness of the H feature dimmed by 20%. An aerosol model structure consisting of bright $0.25\text{-}\mu\text{m}$ particles uniformly distributed between 1 and 200 mbar is consistent with

Fig. 6. Images of Jupiter's thermal emission at $17.8\text{-}\mu\text{m}$ (left) and $13.0\text{-}\mu\text{m}$ (right), used to sound the 150- and 400-mbar levels, respectively. The images, identified by the UT date and System III longitude of the central meridian, were chosen to present nearly the same Earth-facing hemisphere to show the evolution of tropospheric temperatures at several impact sites over time.

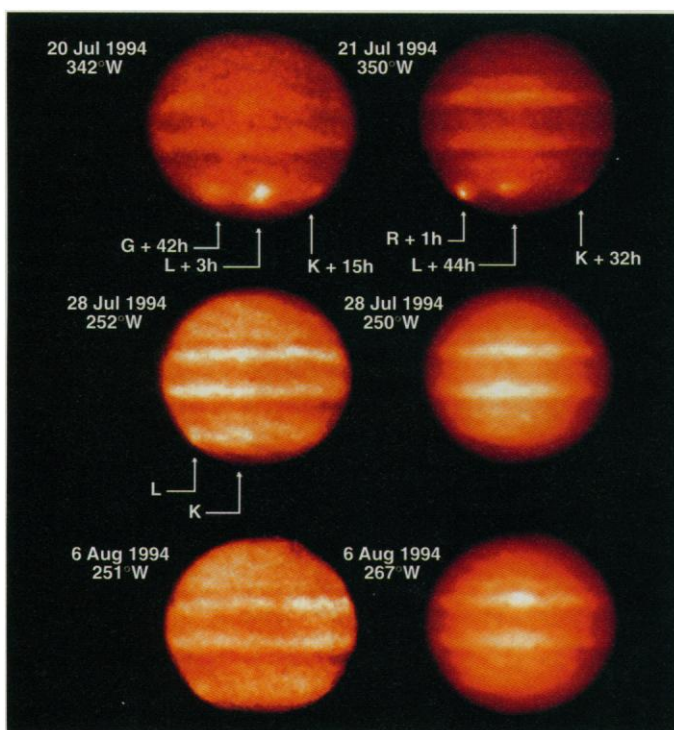


Fig. 7. IRSHELL spectral images of the impact latitudes. The images were created by scanning over the impact sites north and south by 6 arc sec with the 20-arc sec slit oriented parallel to the equator. The two panels are images taken from different portions of the spectrum simultaneously. The upper image was derived from the center of the ν_2 $\text{P}_1(3)$ line of NH_3 at 908 cm^{-1} ; the lower image was derived by averaging the radiance off the line center. Contours on the upper image are shown between radiances of 0.00 and 0.45 and on the lower image between 0.00 to 0.18 at intervals of $0.20\text{ erg s}^{-1}\text{ cm}^{-2}\text{ sr}^{-1}(\text{cm}^{-1})^{-1}$. The strong emission arises from impact site K.

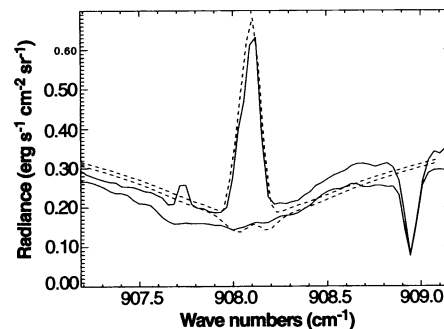
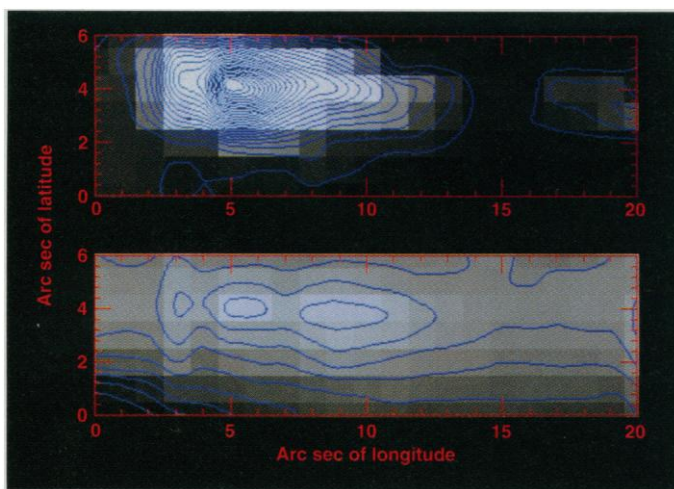


Fig. 8. IRSHELL spectra at the K impact site (upper curves) and 6 arc sec away (lower curves). This is another portion of the data set shown in Fig. 7. Observations are shown in solid and models in dashed curves. The absorption feature at 908.95 cm^{-1} is attributed to absorption in Earth's atmosphere.

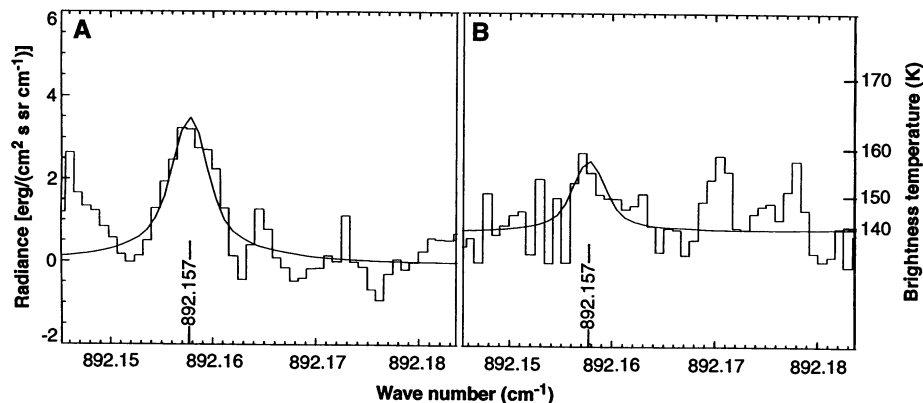


Fig. 9. (A) NH_3 emission line from the stratosphere of Jupiter at the site of the impact of fragment Q1 8.5 days after impact (29 July 1994, 6:21 UT). Measurements were made by the IRHS at 0.00083-cm^{-1} spectral resolution. The spectrum has been smoothed and presented at an effective resolution of 0.00166 cm^{-1} . The solid curve represents the best fit for a temperature profile off the impact site. (B) The same spectral region measured 8° off the Q1 impact site at 6:43 UT.

these infrared brightnesses, as well as visible brightnesses observed by the Hubble Space Telescope (16). In the core of the G feature, the model indicates particle column densities of $(3.0 \pm 0.5) \times 10^8\text{ cm}^{-2}$, corresponding to opacities of 2.4 ± 0.4 at $0.89\text{ }\mu\text{m}$ and 0.085 ± 0.015 at $2.14\text{ }\mu\text{m}$. The Q1 and R impact sites are 30% and 50% dimmer, respectively, than the G impact site at $2.14\text{ }\mu\text{m}$, implying that their aerosol burden is proportionately smaller.

To determine zonal wind speeds, we measured the drift of the relatively compact H and Q1 impact clouds between 28 July and 7 August over several altitudes; these measurements indicate a negative zonal velocity gradient with altitude (a decreasing vertical shear velocity) of $-1.5 \pm 0.8\text{ m s}^{-1}$ (scale height) $^{-1}$, consistent with the prediction from Voyager infrared data (17). Other features underwent considerable expansion during the same period. For exam-

ple, the K impact particulates expanded in longitude at a rate of $6.14 \pm 1.54\text{ m s}^{-1}$.

Aurora

The collision of comet Shoemaker-Levy 9 with Jupiter had a profound effect on the planet's infrared H_3^+ auroral emissions, which have long been used to probe the jovian aurorae and ionosphere (18). Before the impacts and in images taken on 17 July about an hour after the C impact, the emission of the northern and southern aurora were generally similar, with the south being slightly brighter. The northern auroral zone measured at $3.4\text{ }\mu\text{m}$ had an intensity of $1.3 \times 10^{-12}\text{ W m}^{-2}\text{ }\mu\text{m}^{-1}$, compared with the southern aurora at $0.8 \times 10^{-12}\text{ W m}^{-2}\text{ }\mu\text{m}^{-1}$.

However, by the next measurements on

27 July, the northern auroral zone appeared very much brighter than the south (Fig. 11). The northern emission had increased by a factor of nearly 4 to $4.7 \times 10^{-12}\text{ W m}^{-2}\text{ }\mu\text{m}^{-1}$, and the southern aurora was slightly dimmer than it was before impact. Thus, at its peak, the northern emission was six to seven times brighter than the southern emission. Over the next 10 days, the relative and absolute intensities returned to a more normal state. We estimate that dust from the impact latitudes could have migrated into the southern auroral region by 27 July, assuming wind speeds of 50 to 100 m s^{-1} . We are investigating whether the subsequent reduction in conductivity in the south could account for the reduction of H_3^+ emission there while transferring energy to the northern aurora by means of field lines connected through the plasma current sheet (19).

Before the impacts, the north polar stratospheric hot spot, powered by thermalization of high-energy charged particles cascading down magnetic field lines, was located consistently at 60°N , 180°W in System III (20). However, it was not detected during the impacts. It was tentatively visible on 28 July (Fig. 8) but disappeared again, returning on 6 August. If the dust associated with the cometary fragments was responsible for short-term modulations of the electromagnetic environment, we conclude that the time scale associated with generating the polar hot spot is very short.

Remaining Work

Much remains to be done. The search for impact-related atmospheric waves may provide a unique probe of the structure and dynamics of the deep atmosphere. Ac-

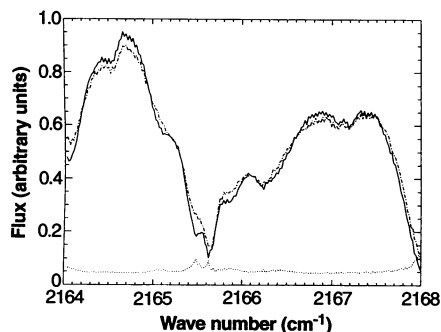


Fig. 10. Spectra of Jupiter made with CSHELL on 2 August 1994. The spectral scale is approximate and the flux scale is arbitrary. The solid line shows a spectrum near the CO 1-0 R5 line with the slit centered along the impact latitude at 45°S , and the dashed-dotted curve shows a spectrum taken at 45°N . The dotted curve shows the ratio of the two spectra scaled upward by a factor of 1000.

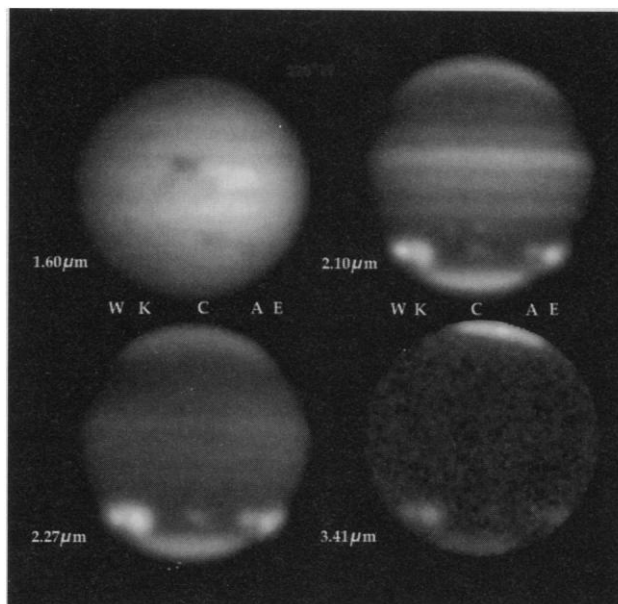


Fig. 11. Images of Jupiter taken with NSFCAM on 27 July 1994. The images are logarithmically stretched to show the greatest dynamic range. The images were taken near 8:28 UT when the central meridian was 228°W in System III. In this sequence of figures, the atmospheric gaseous absorption increases monotonically with wavelength. Only the highest particulates reflect sunlight in the $3.41\text{-}\mu\text{m}$ image, which is otherwise dominated by H_3^+ aurora at the poles and a faint airglow over the planet as a whole.

curate photometric and geometric calibration and intercomparison of the atmospheric experiment results will provide the strongest possible constraints on atmospheric properties, even for regions of the planet not affected by the impacts. Collaborations with other observers will also fill in spectral, spatial, and temporal gaps in coverage. These data will be used to refine models of the jovian system, particularly the atmosphere, and will be used to support the interpretation of observations made by the Galileo mission at Jupiter.

REFERENCES AND NOTES

1. Selection of science goals was made by science team members M. A'Hearn, K. Baines, D. Deming, T. Dowling, C. Griffith, J. Goguen, H. Hammel, W. Hoffmann, D. Hunten, D. Jewitt, T. Kostiuk, S. Miller, K. Noll, G. Orton (chair), and K. Zahnle.
2. These include atmospheric inertia-gravity waves [J. Harrington, R. P. LeBeau, K. A. Backes, T. E. Dowling, *Nature* **368**, 525 (1994)], internal seismic waves [M. Marley, *Astrophys. J. Lett.* **427**, L63 (1994)]; found with a search method presented in D. H. Hunten, W. F. Hoffmann, A. L. Sprague, *Geophys. Res. Lett.* **1**, 1091 (1994)], and trapped oscillations (p -modes) induced by the collisions. We will report on these investigations elsewhere.
3. J. Rayner *et al.*, *Proc. SPIE* **1946**, 490 (1993).
4. T. Greene, A. T. Tokunaga, D. W. Toomey, J. S. Carr, *ibid.*, p. 313. Both NSFCAM and CSHELL are IRTF facility instruments that used 256 by 256 detector arrays.
5. W. F. Hoffmann, G. G. Fazio, K. Shivanandan, J. L. Hora, L. K. Deutsch, *Proc. SPIE* **1946**, 449 (1993); *Infrared Phys. Technol.* **35**, 175 (1994). MIRAC2 was constructed and is operated by Steward Observatory, University of Arizona, and the Smithsonian Astrophysical Observatory. It was commissioned on 13 July 1994 with a 128 by 128 detector Si:As array, which was used between 2 and 21 μm .
6. J. Lacy *et al.*, *Publ. Astron. Soc. Pac.* **101**, 1166 (1989). IRSHELL is operated by the University of Texas at Austin. A 20 by 64 detector array in IRSHELL, used between 7 and 17 μm , was first used on 19 July.
7. T. Kostiuk and M. J. Mumma, *Appl. Opt.* **22**, 2644 (1983); T. Kostiuk, *Infrared Phys. Technol.* **35**, 243 (1994). Both the IRHS technique and its application to planetary atmospheric studies are described in these papers. The IRHS is capable of measuring the shapes of spectroscopic lines emitted by Jupiter's stratosphere.
8. D. Jewitt and P. Kalas, communication posted to the Shoemaker-Levy 9 electronic bulletin board (Planetary Data System Small Bodies Node, University of Maryland), 19 July 1994.
9. H. B. Hammel *et al.*, *Science* **267**, 1288 (1995).
10. J. R. Graham, I. De Pater, J. Garrett Jernigan, M. C. Liu, M. E. Brown, *ibid.*, p. 1320; P. D. Nicholson *et al.*, *Geophys. Res. Lett.*, in press. The arrival times of the first signals detected by the Palomar and Keck telescopes agree to within 7 s.
11. G. S. Orton *et al.*, *Science* **252**, 537 (1991); G. S. Orton *et al.*, *ibid.* **265**, 625 (1994).
12. M. Flasar, in *Time-Variable Phenomena in the Jovian System*, M. Belton, G. Hunt, R. West, Eds. (NASA Spec. Publ. 494, National Aeronautics and Space Administration, Washington, DC, 1986), p. 324.
13. G. Orton, J. Lacy, A. Castillo, J. Achtermann, P. Parmar, *Bull. Am. Astron. Soc.* **24**, 1041 (1992).
14. T. Kostiuk, F. Espenak, M. J. Mumma, D. Deming, D. Zipoy, *Icarus* **72**, 394 (1987); T. Livengood, T. Kostiuk, F. Espenak, J. Goldstein, *J. Geophys. Res.* **98**, 18813 (1993).
15. The temperature near 1 μbar was determined to be 200 ± 50 K from the Voyager 2 Ultraviolet Spectrometer α Leo occultation experiment [S. K. Atreya, T. Donahue, M. C. Festou, *Astrophys. J.* **247**, L43 (1981); M. C. Festou *et al.*, *J. Geophys.*

- Res.* **86**, 5715 (1981)].
16. R. West *et al.*, *Science* **267**, 1296 (1995).
17. P. J. Gierasch, B. J. Conrath, J. A. Magalhaes, *Icarus* **67**, 456 (1986).
18. P. Drossart *et al.*, *Nature* **340**, 539 (1989).
19. S. Miller *et al.*, *Geophys. Res. Lett.*, in press.
20. S. J. Kim, *Icarus* **75**, 399 (1988); J. Caldwell, A. T. Tokunaga, G. S. Orton, *ibid.* **53**, 133 (1983).
21. We thank the engineering staff of the IRTF, headed by P. Jensen, for their support in making so many late improvements to the telescope performance possible. This research was sponsored by various grants from NASA and NSF for work performed at each of the institutions with which the authors of this paper are associated. The MIRAC2 upgrade to the 128 \times 128 array was also supported by Stew-

ard Observatory, University of Arizona, and Smithsonian Astrophysical Observatory. T.L. was a National Research Council Resident Research Associate. M.A'H., K.B., A.D., L.D., F.E., P.E., K.F., J.F., J. Goguen, C.G., H.H., J. Harrington, W.H., J. Hora, D.H., D.K., R.K., T. Kostiuk, J.L., C.L., S.M., K.N., G.O., A.S., K.W., P.Y.-F., K.Z., and D.Z. were visiting astronomers at IRTF, which is operated by the University of Hawaii under contract to NASA. We thank Research Systems, Inc., for donating several licenses for the Interactive Data Language (IDL), which was used to generate most of the graphics in this paper. B. Taylor is gratefully acknowledged for data reduction support, as are C. Lachata and S. Benskin for color photographic services.

The Hubble Space Telescope (HST) Observing Campaign on Comet Shoemaker-Levy 9

H. A. Weaver,* M. F. A'Hearn, C. Arpigny, D. C. Boice, P. D. Feldman, S. M. Larson, P. Lamy, D. H. Levy, B. G. Marsden, K. J. Meech, K. S. Noll, J. V. Scotti, Z. Sekanina, C. S. Shoemaker, E. M. Shoemaker, T. E. Smith, S. A. Stern, A. D. Storrs, J. T. Trauger, D. K. Yeomans, B. Zellner

The Hubble Space Telescope made systematic observations of the split comet P/Shoemaker-Levy 9 (SL9) (P designates a periodic comet) starting in July 1993 and continuing through mid-July 1994 when the fragments plunged into Jupiter's atmosphere. Deconvolutions of Wide Field Planetary Camera images indicate that the diameters of some fragments may have been as large as ~ 2 to 4 kilometers, assuming a geometric albedo of 4 percent, but significantly smaller values (that is, < 1 kilometer) cannot be ruled out. Most of the fragments (or nuclei) were embedded in circularly symmetric inner comae from July 1993 until late June 1994, implying that there was continuous, but weak, cometary activity. At least a few nuclei fragmented into separate, condensed objects well after the breakup of the SL9 parent body, which argues against the hypothesis that the SL9 fragments were swarms of debris with no dominant, central bodies. Spectroscopic observations taken on 14 July 1994 showed an outburst in magnesium ion emission that was followed closely by a threefold increase in continuum emission, which may have been caused by the electrostatic charging and subsequent explosion of dust as the comet passed from interplanetary space into the jovian magnetosphere. No OH emission was detected, but the derived upper limit on the H_2O production rate of $\sim 10^{27}$ molecules per second does not necessarily imply that the object was water-poor.

The Hubble Space Telescope (HST) first observed the periodic comet SL9 on 1 July 1993 (1). After the successful HST servicing mission in December 1993, the HST began observing SL9 again in January 1994 and monitored the comet until its impact into Jupiter in mid-July (Table 1).

Because of the large spatial extent of SL9 in 1994 and the relatively small fields of view of the HST cameras, the only time that the HST observed the entire "train" of fragments during 1994 was on 17 May. Figure 1 shows the composite SL9 image created from some images taken on this date with the Wide Field Planetary Camera 2 (WFPC2) (2) and identifies the fragments

with their letter labels. Fragment A was the first to impact Jupiter (on 16 July 1994) and nucleus W was the last (on 22 July 1994). The apparent separation of fragments A and W increased by a factor of ~ 5 (from 70 to 360 arc sec) between the time of the first HST images taken on 1 July 1993 and the ones taken on 17 May 1994.

Although a total of 39 orbits of HST observing time was devoted to imaging of the comet (3), this was not nearly enough to provide detailed temporal coverage on all the fragments. We focused our attention on three different portions of SL9: the regions around the complex of fragments P and Q, the S fragment, and the G fragment. All of